AIP Journal of Applied Physics

Investigation of the impact of insulator material on the performance of dissimilar electrode metal-insulator-metal diodes

Nasir Alimardani, Sean W. King, Benjamin L. French, Cheng Tan, Benjamin P. Lampert, and John F. Conley Jr.

Citation: Journal of Applied Physics **116**, 024508 (2014); doi: 10.1063/1.4889798
View online: http://dx.doi.org/10.1063/1.4889798
View Table of Contents: http://scitation.aip.org/content/aip/journal/jap/116/2?ver=pdfcov
Published by the AIP Publishing

Articles you may be interested in

Conduction processes in metal–insulator–metal diodes with Ta2O5 and Nb2O5 insulators deposited by atomic layer deposition
J. Vac. Sci. Technol. A **32**, 01A122 (2014); 10.1116/1.4843555

Impact of top electrode on electrical stress reliability of metal-insulator-metal capacitor with amorphous ZrTiO 4 film
Appl. Phys. Lett. **96**, 133501 (2010); 10.1063/1.3377914

Influence of the electrode material on Hf O 2 metal-insulator-metal capacitors
J. Vac. Sci. Technol. B **27**, 286 (2009); 10.1116/1.3071843

High-temperature conduction behaviors of HfO 2 / TaN -based metal-insulator-metal capacitors
J. Appl. Phys. **102**, 073706 (2007); 10.1063/1.2786712

Thin film solid-state reactions forming carbides as contact materials for carbon-containing semiconductors
J. Appl. Phys. **101**, 053714 (2007); 10.1063/1.2561173

AIP Journal of Applied Physics

Journal of Applied Physics is pleased to announce André Anders as its new Editor-in-Chief

[This article is copyrighted as indicated in the article. Reuse of AIP content is subject to the terms at: http://scitation.aip.org/termsconditions. Downloaded to] IP: 128.193.38.25 On: Mon, 14 Jul 2014 16:34:45

JOURNAL OF APPLIED PHYSICS **116**, 024508 (2014)

Investigation of the impact of insulator material on the performance of dissimilar electrode metal-insulator-metal diodes

Nasir Alimardani,[1] Sean W. King,[2] Benjamin L. French,[3] Cheng Tan,[1] Benjamin P. Lampert,[1] and John F. Conley, Jr.[1,a)]
[1]*School of Electrical Engineering and Computer Science, Oregon State University, Corvallis, Oregon 97331, USA*
[2]*Logic Technology Development, Intel Corporation, Hillsboro, Oregon 97124, USA*
[3]*Ocotillo Materials Laboratory, Intel Corporation, Chandler, Arizona 85248, USA*

(Received 18 April 2014; accepted 2 June 2014; published online 14 July 2014)

The performance of thin film metal-insulator-metal (MIM) diodes is investigated for a variety of large and small electron affinity insulators using ultrasmooth amorphous metal as the bottom electrode. Nb_2O_5, Ta_2O_5, ZrO_2, HfO_2, Al_2O_3, and SiO_2 amorphous insulators are deposited via atomic layer deposition (ALD). Reflection electron energy loss spectroscopy (REELS) is utilized to measure the band-gap energy (E_G) and energy position of intrinsic sub-gap defect states for each insulator. E_G of as-deposited ALD insulators are found to be $Nb_2O_5 = 3.8\,eV$, $Ta_2O_5 = 4.4\,eV$, $ZrO_2 = 5.4\,eV$, $HfO_2 = 5.6\,eV$, $Al_2O_3 = 6.4\,eV$, and $SiO_2 = 8.8\,eV$ with uncertainty of $\pm 0.2\,eV$. Current vs. voltage asymmetry, non-linearity, turn-on voltage, and dominant conduction mechanisms are compared. Al_2O_3 and SiO_2 are found to operate based on Fowler-Nordheim tunneling. Al_2O_3 shows the highest asymmetry. ZrO_2, Nb_2O_5, and Ta_2O_5 based diodes are found to be dominated by Frenkel-Poole emission at large biases and exhibit lower asymmetry. The electrically estimated trap energy levels for defects that dominate Frenkel-Poole conduction are found to be consistent with the energy levels of surface oxygen vacancy defects observed in REELS measurements. For HfO_2, conduction is found to be a mix of trap assisted tunneling and Frenkel-Poole emission. Insulator selection criteria in regards to MIM diodes applications are discussed. © *2014 AIP Publishing LLC*.
[http://dx.doi.org/10.1063/1.4889798]

I. INTRODUCTION

Thin film metal-insulator-metal (MIM) tunnel devices have experienced a renewal in interest for ultra-high-speed applications such as hot electron transistors,[1,2] diodes for optical rectenna based infrared (IR) energy harvesting,[3,4] and IR detectors,[5,6] as well as for selector diodes for resistive random access memory (RRAM),[7,8] and MIM tunnel emission cathodes.[9,10] Because of their simple structure and low temperature processing, MIM building blocks are also being considered for large area macroelectronics such as liquid crystal display (LCD) backplanes.[11,12] For many of these applications, figures of merit include high asymmetry, strong nonlinearity, and fast responsivity of current vs. voltage (I-V) behavior at low voltages.

The standard approach to achieving high speed rectification in an MIM device is based on Fowler-Nordheim tunneling (FNT) conduction in conjunction with the use of dissimilar work function metal electrodes (where $\Phi_{M1} \neq \Phi_{M2}$) to produce an asymmetric, polarity dependent electron tunneling barrier.[13] FNT conduction is exponentially dependent upon the metal/insulator barrier height, electric field, and insulator thickness. The uniformity of the electric field is critical. Attention must therefore be paid to metal/insulator interface roughness as well as insulator quality.

Although many investigations of MIM tunnel diodes have been reported over the years, the majority of these studies were adversely affected by two technological limitations. The first limitation of previous studies is that they made use of inherently rough polycrystalline metal bottom electrodes. The as-deposited roughness of poly-crystalline metal films can be several times larger than the tunnel barrier thickness. It has been theoretically predicted that interfacial roughness can influence the tunneling current across junctions[14] and we experimentally demonstrated that roughness of the bottom metal electrode can overwhelm the influence of work function difference ($\Delta\Phi_M$) on MIM current-voltage (I-V) characteristics as well as deteriorate device yield.[15–17] The second limitation of most previous experimental investigations of MIM diodes is that they focused on the use of insulators produced by oxidation or nitridation of these underlying polycrystalline metal electrodes.[5,6,10,18–20] Insulators formed in this manner are typically of low quality which can have a severe negative impact on device performance and repeatability.

Thus, although it appears that much work has been reported on thin film MIM diodes, these studies have involved primarily low quality oxides or nitrides of the polycrystalline bottom metal electrode and have resulted in poor characteristics or repeatibilty.[18–20] In addition, the practice of using native oxides and nitrides strictly limits the range of metal-insulator combinations that can be studied. To target different applications, it is desirable to pair up insulators having a range of band-gaps and electron affinities with small and large work

[a)]Author to whom correspondence should be addressed. Electronic mail: jconley@eecs.oregonstate.edu.

 © 2014 AIP Publishing LLC

[This article is copyrighted as indicated in the article. Reuse of AIP content is subject to the terms at: http://scitation.aip.org/termsconditions. Downloaded to] IP: 128.193.38.25 On: Mon, 14 Jul 2014 16:34:45

function metals. For example, insulators with large electron affinities (low barrier heights), such as Nb_2O_5 and Ta_2O_5, are potential candidates for rectenna based IR energy harvesting applications which must operate in a very low bias regime.[4,20] On the other hand, Al_2O_3 and SiO_2 with relatively large band-gaps and small electron affinity values are desired candidates for liquid crystal display backplanes and their use is already well established in the display industry. HfO_2 and ZrO_2 have intermediate band-gaps and electron affinities and HfO_2 is now used in gate dielectrics in complementary metal-oxide-semiconductor (CMOS) transistors. HfO_2 and Ta_2O_5 are both promising RRAM materials.[21,22] Despite the importance of the insulator in determining MIM performance, a systematic study of the impact on thin film diode performance of various insulators using a fixed electrode pair has not been conducted.

We have shown previously that using atomic layer deposition (ALD) of Al_2O_3 on atomically smooth (0.3 nm RMS with 3 nm peak roughness) bottom metal electrodes large area high quality MIM diodes with well controlled FNT can be realized.[16,17] ALD is based on self-saturating reactions, allowing for high conformality, precise thickness control, and uniformity over large surface areas. An additional benefit of ALD is that it allows deposition of a wide range of high quality insulators independent of the bottom electrode material.[23]

In this work, MIM devices fabricated on ultra-smooth ZrCuAlNi (ZCAN) amorphous metal bottom electrodes using Nb_2O_5, Ta_2O_5, ZrO_2, HfO_2, Al_2O_3, and SiO_2 amorphous insulators deposited via ALD are investigated. MIM diode performance, including current vs. voltage asymmetry, non-linearity, and dominant conduction mechanism is compared as a function of temperature. Reflection electron energy loss spectroscopy (REELS) is utilized to measure the band-gap energy and energy position of sub-gap defect states for each of these insulators. The REELS measured band-gaps are used in the analysis of conduction mechanisms and the energy position of sub-band gap defect states are compared with electrical estimates of trap energy levels. Finally, insulator selection criteria are discussed with regard to potential applications.

II. EXPERIMENTAL

Si coupons coated with a 100 nm thick film of thermally grown SiO_2 were used as starting substrates for MIM device fabrication. ZCAN amorphous metal was selected as the bottom electrode (M_1) due to its atomically smooth as-deposited surface (RMS roughness ~ 0.3 nm).[16,24] Using an ultra-smooth bottom electrode ensures that conduction is not dominated by "hot spots" due to field enhancement at surface topography.[15] ZCAN was deposited via DC magnetron sputtering using a $Zr_{40}Cu_{35}Al_{15}Ni_{10}$ metal target with no intentional substrate heating. Thin insulator tunnel barriers, with the exception of SiO_2, were deposited via ALD in a Picosun SUNALE R-150B chamber at a temperature of 250 °C using deionized water as the oxidant. Metal precursors used were niobium ethoxide for Nb_2O_5, tantalum ethoxide for Ta_2O_5, tetrakis (ethylmethylamino) zirconium (TEMAZr) for ZrO_2, tetrakis (ethylmethylamino) hafnium (TEMAHf) for HfO_2, and trimethylaluminum (TMA) for Al_2O_3. The SiO_2 films were deposited in a Cambridge NanoTech Fiji plasma enhanced atomic layer deposition (PEALD) tool using tris (dimethylamino) silane ($[(CH_3)_2N]_3SiH$) and an O_2 remote plasma at a substrate temperature of 250 °C. Insulator thicknesses of 10 nm were chosen to suppress direct tunneling so as to more easily distinguish FNT conduction. Aluminum dots (~0.2 mm^2), thermally evaporated through a shadow mask, were used as the top electrode (M_2).

The thicknesses of insulator films deposited on Si were measured with a J.A. Woollam WVASE32 spectroscopic ellipsometer using a Cauchy model. Spectroscopic ellipsometry was also used to measure the index of refraction, n, in the wavelength range of 400–1200 nm in order to estimate the optical dielectric constant (n^2).

Using electron beam and X-ray diffraction (XRD), it was determined that all ALD films were amorphous as-deposited. Crystalline phases in insulator films may create conduction paths for electrons and thus facilitate defect-dominated leakage mechanisms.[25] Likewise, crystallization of bottom electrode increases electrode surface roughness which can generate local electric field enhancements or hot spots.[26] Atomic force microscopy (AFM) shows an increase in surface roughness and XRD shows signs of crystallization when ZCAN is annealed at 380 °C and above. In order to avoid the possibility of crystallization of either the ALD insulators or the ZCAN bottom electrodes, all devices are studied as-deposited, without annealing treatments.

A Kelvin probe electrostatic voltmeter was used to determine metal electrode work functions. The work function of the ZCAN electrode (Φ_{ZCAN}) was found to be approximately 4.8 eV and the difference between the ZCAN and Al work functions ($\Delta\Phi = \Phi_{ZCAN} - \Phi_{Al}$) was approximately 0.6 eV. These values were confirmed by the extrapolation of Fowler-Nordheim plots, reported in detail elsewhere.[27]

Dielectric constants were determined using capacitive vs. voltage (C-V) measurements taken on an Agilent B1500 semiconductor device parameter analyzer. Room temperature I-V measurements were performed on a probe station in a dark box using an Agilent 4156C semiconductor parameter analyzer; the noise floor of this system is estimated to be on the order of 100 pA. All I-V measurements at temperatures ranging from 25 to 100 °C were conducted using a Temptronic gold plated ThermoChuck and a probe station in a dark box. I-V measurements below the room temperature were performed in a LakeShore EMPX-HF cryogenic probe station. I-V measurements were performed with the ZCAN bottom electrode (M_1) held at ground and with bias applied to the Al top gate (M_2). To mitigate the impact of displacement current, all I-V curves were swept from zero bias to either the maximum positive or negative bias. We define the turn-on bias (V_{ON}) as the bias at which current begins to increase exponentially with voltage. Two key figures of merit are defined to characterize the devices. I-V asymmetry, $\eta_{asym.}$, is defined as negative current divided by positive current $|I_-/I_+|$, so that $\eta_{asym} = 1$ indicates symmetric operation. Non-linearity, f_{NL}, is defined as $(dI/dV)/(I/V)$.

A VG 350 Auger electron spectroscopy system was used for REELS analysis to estimate band-gaps and defect levels. The details of the system and REELS experiments have been

[This article is copyrighted as indicated in the article. Reuse of AIP content is subject to the terms at: http://scitation.aip.org/termsconditions. Downloaded to] IP: 128.193.38.25 On: Mon, 14 Jul 2014 16:34:45

reported elsewhere.[28,29] Briefly, the oxide dielectrics were transferred *ex-situ* to the REELS system and spectra were collected using 0.5 and 2.5 keV primary electron beam energies. The hemispherical electron energy analyzer was operated at a resolution of 0.2 eV with a pass energy of 8 eV. A shallow surface exit angle of 80° relative to the surface normal was used to improve surface sensitivity and reduce the background intensity from inelastically scattered electrons in the low-energy tail of the primary elastic peak. The band-gaps of the oxide dielectrics were estimated from the raw REELS spectra by linearly extrapolating the leading edge of the electron energy loss spectrum to the elastic peak baseline. A 3-keV Ar^+ ion sputtering beam operated at 10 $\mu A/cm^2$ was additionally utilized to remove surface contamination from *ex-situ* transfer and induce surface defects. Features detected in the REELS spectra below the band-gap energy were treated as either extended states arising from the amorphous structure of the oxide dielectrics or more specific defect states.

Band diagrams were simulated using the Boise State University Band Diagram program.[30] Materials parameters used in simulations are based on Kelvin probe and REELS measurements as well as literature values reported for ALD insulators deposited using the same precursors and process temperatures.

III. RESULTS AND DISCUSSION

A. REELS investigations

Shown in Fig. 1 are REELS spectra taken from both as-deposited and Ar^+ sputtered 10 nm thick ALD films of (a) SiO_2, (b) Al_2O_3, (c) HfO_2, (d) ZrO_2, (e) Ta_2O_5, and (f) Nb_2O_5, each on 150 nm thick ZCAN metal films on Si. As illustrated in each figure, the band-gaps were estimated via linear extrapolation of the leading edge of the loss for each ALD film. Defect levels were determined from the loss peaks that appeared after Ar^+ sputtering.[28,29]

As has been previously reported for PECVD and thermal SiO_2,[29,31] a large surface band-gap of 8.8 ± 0.2 eV was observed for the as-deposited PEALD SiO_2 film and Ar^+ sputter induced surface oxygen vacancy (SOV) defect centers were observed to appear in the band-gap at ~5.0 and 7.2 eV. Smaller band-gaps of 5.4–6.6 eV were observed for as-deposited Al_2O_3, HfO_2, and ZrO_2, where Ar^+ sputtering was also observed to induce surface oxygen vacancy related defect centers in the band-gap.[31] For Al_2O_3, the surface band-gap of 6.4 ± 0.2 eV is substantially reduced relative to the value of 7.8 eV typically quoted for sapphire and has been previously attributed to the presence of residual hydrogen, organics, and a slight non-stoichiometry in the ALD deposited film.[31] Similar to SiO_2, Ar^+ sputtering of Al_2O_3 induces surface oxygen vacancy defect centers just below the conduction band minimum centered at approximately 5.0 eV.

HfO_2 and ZrO_2 exhibit similar band-gaps of 5.6 ± 0.2 and 5.4 ± 0.2 eV, respectively. The Ar^+ sputter induced defects states for HfO_2 and ZrO_2 were also similar and exhibited a broader distribution deeper in the band-gap (centered at approximately 2–2.5 eV above the elastic peak and extending up to the conduction band edge). These Ar^+ sputter induced defect centers have been previously observed in photoemission experiments by Morant[32] for ZrO_2 and are consistent with the oxygen vacancy defect centers modeled by Robertson[33] and Foster[34,35] for both ZrO_2 and HfO_2. In contrast, electrical and spectroscopic ellipsometry measurements have observed the presence of shallower trap and defect states distributed at 0.3–1.2 eV below the HfO_2 conduction band minimum.[36–39] However, this is still consistent with the REELS measurements where the distribution of Ar^+ sputter induced defects (centered at 3.4 eV below the conduction band) extends up to the conduction band minimum.

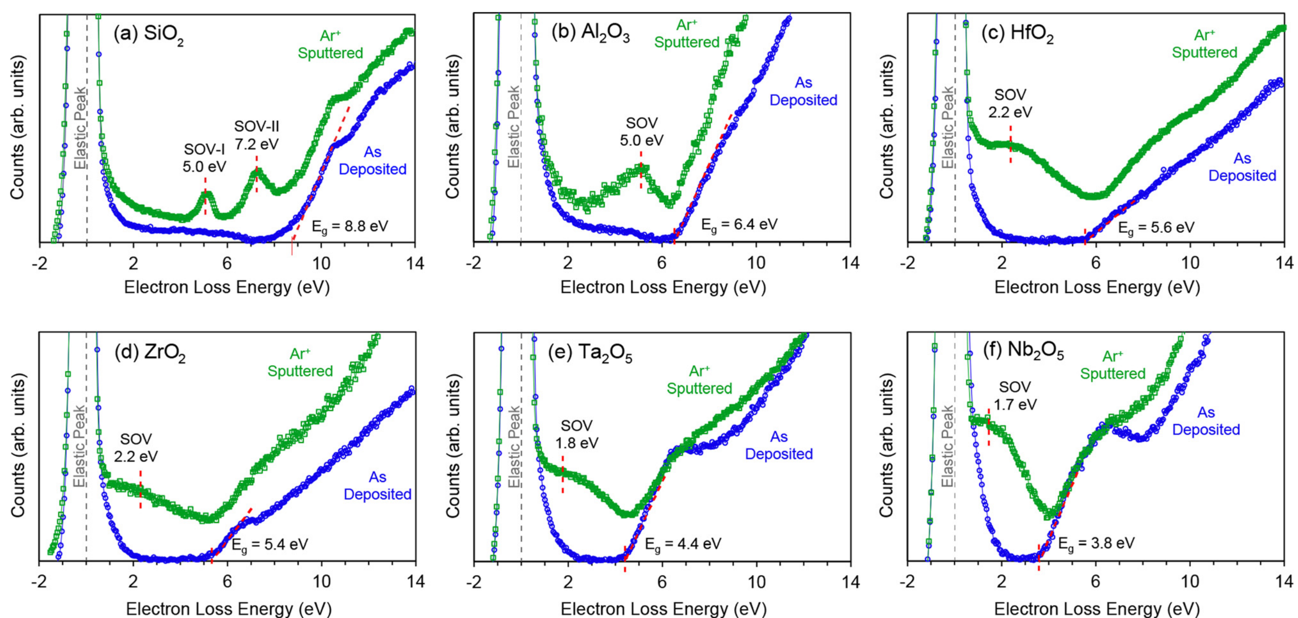

FIG. 1. REELS spectra of as-deposited and Ar^+ sputtered thin films of (a) SiO_2, (b) Al_2O_3, (c) HfO_2, (d) ZrO_2, (e) Ta_2O_5, and (f) Nb_2O_5. The intersection of the gray dashed lines indicates the onset of the loss spectrum for the purpose of calculating the band-gap energy. Peaks in the post Ar^+ sputtered films indicate distinct defect levels.

[This article is copyrighted as indicated in the article. Reuse of AIP content is subject to the terms at: http://scitation.aip.org/termsconditions. Downloaded to] IP: 128.193.38.25 On: Mon, 14 Jul 2014 16:34:45

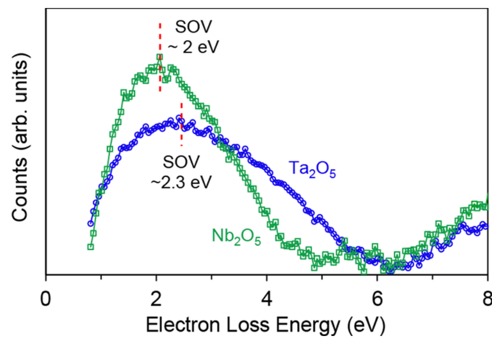

FIG. 2. Plot of the difference between the post Ar^+ sputtering and as-deposited REELS spectrums for Nb_2O_5 and Ta_2O_5.

In this regard, it is important to note that the Ar^+ sputter induced sub-gap defect states detected in REELS are primarily located within a few atomic layers of the surface and likely exhibit a different range of valence states relative to the distribution of related bulk traps/defects in the ALD oxide dielectric. Therefore, it is plausible that the REELS defects in the upper part of the Ar^+ sputter induced defect tail are more directly related to the electrically and optically detected trap / defect states.

Analysis of the REELS spectra from as-deposited Ta_2O_5 and Nb_2O_5 indicated substantially smaller band-gaps of 4.4 ± 0.2 and 3.8 ± 0.2 eV, respectively. Similar to the other oxide dielectrics investigated, Ar^+ sputtering was also observed to create defect states in the band-gap of Ta_2O_5 and Nb_2O_5 that based on analogy are also believed to be surface oxygen vacancies. However, the defect states for Ta_2O_5 and Nb_2O_5 do not show a clear maximum in peak intensity. They are instead manifested as a broad tail below the elastic peak that merges with the turn-on in electron energy loss due to exciton creation and promotion of valence band electrons into the conduction band. To more clearly see the position of the Ar^+ sputter induced defects, the as-deposited REELS spectra for Ta_2O_5 and Nb_2O_5 were subtracted from their respective Ar^+ sputter spectra. As shown in Fig. 2, the resulting difference spectra show a high concentration of defect states at low loss energy with a slight peak in electron energy loss at 2.0 eV for Nb_2O_5 and 2.3 eV for Ta_2O_5 that gradually decreases to zero as the band-gap energy is approached. As mentioned previously, the broad distribution of surface defects states observed in REELS is likely due to the range of different valence states produced by the Ar^+ sputtering of ionic materials. In this regard, the REELS results are qualitatively most consistent with prior theoretical studies of oxygen vacancy defects in Ta_2O_5 that have shown the V_O^{1+} defect to lie at 0.8–1.5 eV below the conduction band minimum.[40,41]

The results of the REELS band-gap and defect level measurements are summarized in Table I. Also included in Table I are electrically extracted trap levels (discussed in Sec. III B), electron affinities, χ, dielectric constant (κ), index of refraction, n, and optical dielectric constant, n^2. Trap levels are referenced to the conduction band edge. The electron affinity values of the insulators are reported values for ALD insulators deposited using the same or similar ALD precursors and process temperatures. Dielectric constant values are acquired by C-V measurements on the as-deposited ALD films using thickness values measured by ellipsometry. Spectroscopic ellipsometry was used to measure n. The parameters in this table are used in simulations of conduction mechanisms in Sec. III B.

B. Electrical properties of MIM diodes

Room temperature log current density (J)-V curves of ZCAN/insulator/Al MIM diodes made with 10 nm of either SiO_2, Al_2O_3, HfO_2, ZrO_2, Ta_2O_5, or Nb_2O_5 are shown in Fig. 3(a). The maximum voltage sweep range for each diode is chosen to be a few 100 mV below the breakdown field of the respective insulator. Band diagrams of each MIM diode are presented in Fig. 3(b) and are based on the materials properties tabulated in Table I. Looking at Fig. 3, it is seen that the I-V responses of the diodes is qualitatively related to the relative band-gaps and band offsets of the insulators—the smaller the band gap, the larger the current response and the lower the turn on voltage, V_{ON}. Diodes made with SiO_2, which has the largest band gap, show the smallest current conduction, whereas the Nb_2O_5 diodes, having the narrowest E_G/largest χ insulator, exhibit the largest current conduction. The metal-insulator barrier heights, calculated based on measurements of the metal work functions and reported values of insulator electron affinities, predict well V_{ON} of the diodes where $V_{ON\text{-}Nb2O5} < V_{ON\text{-}Ta2O5} < V_{ON\text{-}ZrO2} < V_{ON\text{-}HfO2} < V_{ON\text{-}Al2O3} < V_{ON\text{-}SiO2}$.

A closer look at Fig. 3(a) reveals distinct "knees" in the I-V curves for the SiO_2, Al_2O_3, and HfO_2 diodes at relatively large electric field at both positive and negative polarities. Following the appearance of the knees, the current density increases exponentially for several orders of magnitude with

TABLE I. The electronic properties of ALD thin films studied in this work. All the values summarized in the table except electron affinities have been acquired experimentally in this work. The electron affinity values of the insulators are reported values for ALD insulators deposited using the same (or similar) ALD precursors and process temperatures. Trap energy levels are referenced to the conduction band edge. E_G and Φ_T extracted from REELS have error bars of ± 0.2 eV.

Insulator	E_G (eV)	REELS Φ_T (eV)	Extracted Φ_T (eV)	χ (eV)	κ	n	n^2 (ε_∞)	κ_{FPE}
SiO_2	8.8	3.8, 1.6	…	0.9[42]	4	1.45–1.56	2.1–2.4	…
Al_2O_3	6.4	1.4	…	1.4[43]	7.6	1.58–1.72	2.5–3.0	…
HfO_2	5.6	~0.2–3.6	…	2.25[37]	18	2.06–2.13	4.2–4.5	…
ZrO_2	5.4	~0.2–3.4	1.65 ± 0.1	2.75[44]	22	2.12–2.21	4.4–4.9	4.4 ± 0.1
Ta_2O_5	4.4	~0.2–4.2	0.53 ± 0.05	3.2[45]	24[47]	2.14–2.22	4.6–4.9	4.6 ± 0.1
Nb_2O_5	3.8	~0.2–3.6	0.62 ± 0.05	4[46]	25	2.34–2.49	5.5–6.2	5.5 ± 0.1

[This article is copyrighted as indicated in the article. Reuse of AIP content is subject to the terms at: http://scitation.aip.org/termsconditions. Downloaded to] IP: 128.193.38.25 On: Mon, 14 Jul 2014 16:34:45

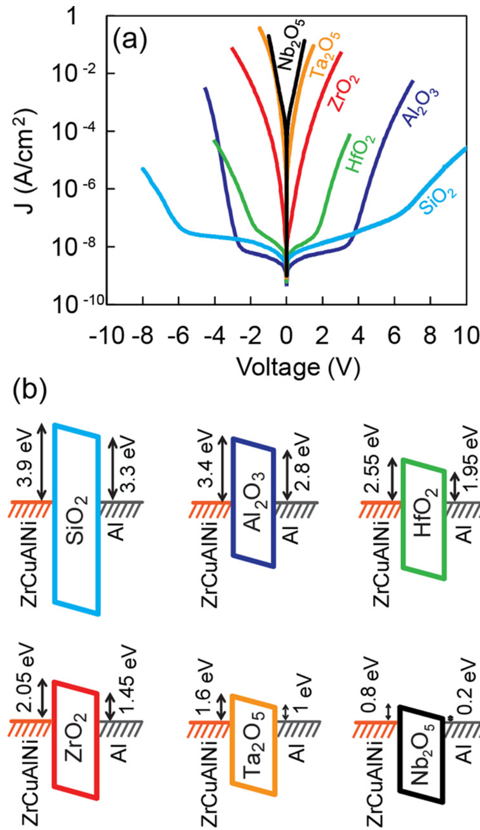

FIG. 3. (a) Plots of log (J) vs. V for M_1IM_2 diodes made on ZrCuAlNi bottom electrodes with 10 nm of either SiO_2, Al_2O_3, HfO_2, ZrO_2, Ta_2O_5, or Nb_2O_5 and Al top electrodes. (b) Simulated band diagrams illustrating these diodes in equilibrium.

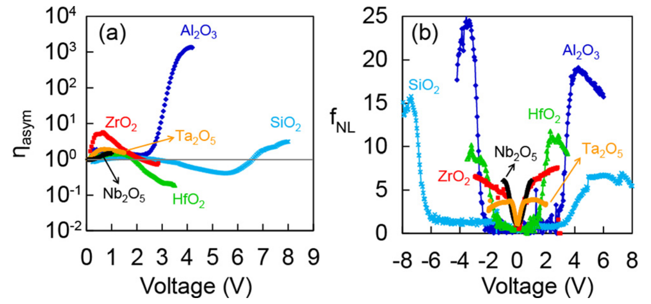

FIG. 4. Plots of (a) log (η_{asym}) and (b) f_{NL} vs. voltage for M_1IM_2 diodes made on ZrCuAlNi bottom electrodes with 10 nm of either SiO_2, Al_2O_3, HfO_2, ZrO_2, Ta_2O_5, or Nb_2O_5, and Al top electrodes.

small increases in applied bias. The knees indicate a change in the dominant conduction mechanism that, as discussed below, is attributed to the onset of FN tunneling dominance. The relative position of the knees corresponds roughly to the relative barrier heights of the diodes, appearing at the lowest voltage for the HfO_2 diodes (smallest barrier) and at the largest voltage for the SiO_2 devices (largest barrier). The ZrO_2, Ta_2O_5, and Nb_2O_5 diodes, on the other hand, do not exhibit knees in their I-V response. These diodes show large leakage current at a very low bias range. The ZrO_2, Ta_2O_5, and Nb_2O_5 insulators all have large electron affinities and thus form small energy barriers with the electrodes, which can allow a thermally activated conduction mechanism such as Schottky emission (SE) to be significant at room temperature.

Two key figures of merit for tunnel diodes are I-V asymmetry (η_{asym}) and non-linearity (f_{NL}). It is often assumed that MIM diodes operate based on FNT. Assuming that conduction is dominated by FNT and neglecting non-idealities such as the formation of metal oxide interfacial layers (ILs), or non-ideal modifications to the effective work function due to the presence of the dielectric,[48] the asymmetry polarity and maximum asymmetry (η_{max}) of M_1IM_2 diodes should be determined primarily by the built in field induced by the vacuum electrode work function difference ($\Delta\Phi_M = \Phi_{M1} - \Phi_{M2}$). In the ideal case, M_1IM_2 diodes with the same top and bottom metal electrodes should exhibit qualitatively similar I-V asymmetry, independent of the tunnel insulator. The η_{asym} and f_{NL} data however, plotted in Fig. 4, suggest that the assumption of FNT dominated conduction is not valid for all insulators. The diodes, in Fig. 4(a), show different asymmetric properties. η_{max} is roughly in order of band-gap. While the Al_2O_3 diode exhibits η_{max} of more than +1500, the ZrO_2, HfO_2, and SiO_2 diodes exhibit η_{max} two orders of magnitude lower with the HfO_2 diodes showing asymmetry of opposite polarity. Note that while the band-gap of SiO_2 is larger than Al_2O_3, the η_{max} of the SiO_2 diode is less than that of Al_2O_3 diode because of two reasons. First, as it is seen in Fig. 3(a), the SiO_2 diodes show larger leakage at low voltages due to deep trap level at 3.8 eV below the conduction band minimum which provides a path for trap assisted tunneling (TAT) at low voltages. Second, as it is seen in Fig. 4(a), at around above 6 V FNT begins to dominate and forward asymmetry increases but before reaching to larger asymmetry values, insulator breakdown occurs. The Ta_2O_5 and Nb_2O_5 diodes are roughly symmetric.

The abrupt changes in f_{NL} with voltage (Fig. 3(b)) are likely due either to changes in the dominant conduction mechanism through the insulator or to charge trapping. The onset voltage of rapidly increasing f_{NL} is correlated roughly with the insulator barrier heights with Ta_2O_5, Nb_2O_5, and ZrO_2 grouped together followed by HfO_2, Al_2O_3, and finally SiO_2. Different maximum values of f_{NL} ($f_{NL\text{-}max}$) are observed.

For diodes dominated by FNT, the bias at which $f_{NL\text{-}max}$ occurs correlates with the onset of FNT and the magnitude of $f_{NL\text{-}max}$ in these devices is an indication of the extent by which FNT dominates these devices. Current due to FNT, I_{FNT}, may be described as

$$I_{FNT} = C_1 \frac{1}{\phi_b} (V)^2 \exp\left(-\frac{C_2 m^{*\frac{1}{2}} \phi_b^{\frac{3}{2}}}{V} \right), \qquad (1)$$

where C_1 and C_2 are universal constants independent of materials properties, ϕ_b is the energy barrier height between the Fermi-level of the injecting electrode and the conduction band minimum of the insulator, m* is the effective electron mass for tunneling electron, and V is voltage.[13,49] To examine whether the dominant conduction process is related to FNT, the room temperature MIM J-V data from Fig. 3(a) were re-plotted as $\ln(I/V^2)$ and (1/V) in Fig. 5. For each device, the bias range for fitting is chosen on the basis of the diode current response. J_{FNT} is exponentially dependent on

[This article is copyrighted as indicated in the article. Reuse of AIP content is subject to the terms at: http://scitation.aip.org/termsconditions. Downloaded to] IP: 128.193.38.25 On: Mon, 14 Jul 2014 16:34:45

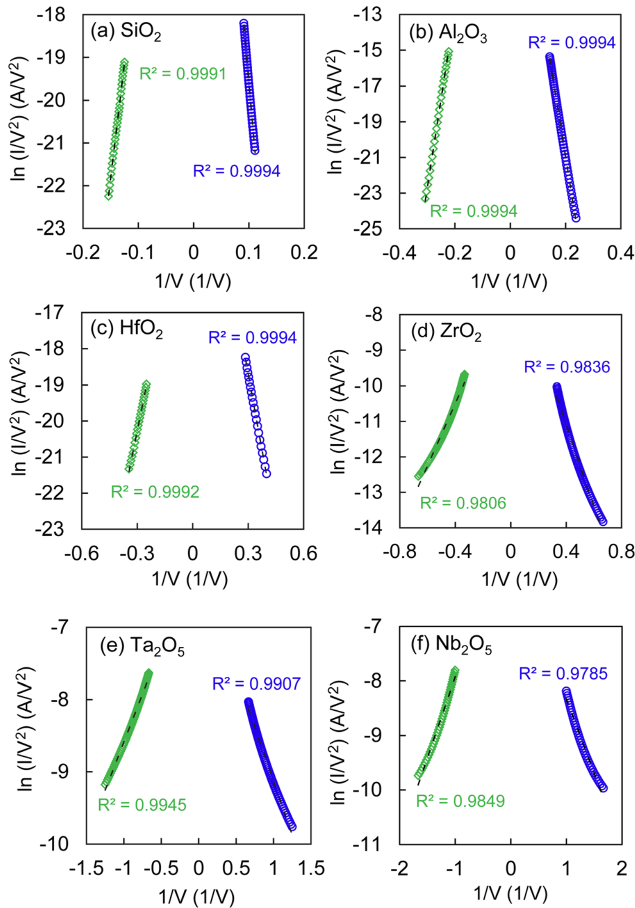

FIG. 5. I-V curves from Fig. 3(a) fitted to FNT plots of ln (I/V^2) vs. 1/V. Green and blue curves represent negative and positive polarities, respectively. Curves showing $R^2 \geq 0.999$ are considered to be highly linear and exhibiting FNT as the dominant conduction mechanism.

the applied voltage and requires high electric fields so that electrons may tunnel into the conduction band of the insulator. For the SiO_2, Al_2O_3, and HfO_2 devices, the voltage range above the occurrence of the V_{ON} "knee" in the log(J)-V plots from Fig. 3(a) were selected. As there is no knee in log(J)-V plots of the ZrO_2, Ta_2O_5, and Nb_2O_5 devices, the J-V curves over the last four orders of magnitude increase in current response were analyzed. A linear relationship between $\ln(I/V^2)$ and (1/V) is an indication that FNT is the dominant conduction mechanism over the bias range. An R^2 value greater than 0.999 was taken to indicate an excellent fit. It is seen in Fig. 5 that the SiO_2, Al_2O_3, and HfO_2 devices all exhibit highly linear $\ln(I/V^2)$ vs. (1/V) curves with $R^2 > 0.999$ for both positive and negative polarities. Thus, for the voltage range defined, FNT is tentatively assigned as the dominant conduction mechanism for the SiO_2, Al_2O_3, and HfO_2 devices. Diodes made with ZrO_2, Ta_2O_5, and Nb_2O_5, however, exhibit poor with R^2 values ranging from 0.98 to 0.99, indicating that FNT does not dominate conduction in these devices.

Besides FNT and direct tunneling (which should be suppressed in the 10 nm thick films), possible competing conduction mechanisms include SE, Frenkel-Poole emission (FPE), and space-charge-limited (SCL) conduction. SCL is ruled out because the current density (J) does not exhibit a V^2 dependence.[50] SE conduction is limited by emission over the energy barrier at the interface. For low energy barrier devices under low bias, SE can be dominant. Current conduction due to Schottky emission, I_{SE}, is described as

$$I_{SE} = A^* T^2 \exp\left[\frac{-q\left(\phi_b - \sqrt{qV/4\pi\kappa_r\varepsilon_0}\right)}{kT}\right], \quad (2)$$

where A* is the effective Richardson constant, T is temperature, q is the elementary charge, κ_r is the optical dielectric constant, ε_0 is the permittivity of free space, and k is Boltzmann's constant.[49] To assess the contribution of SE, the high field J-V data from Fig. 3(a) were replotted as $\ln(I/T^2)$ vs. $V^{1/2}$. A linear relationship between $\ln(I/T^2)$ and $V^{1/2}$ is an indication that SE is dominant. None of these plots (not shown here) demonstrate good linear fits. Hence, SE is not found to dominate conduction mechanism in the high field regime. Note that we previously showed that SE dominates both Ta_2O_5 and Nb_2O_5 in the low bias regime.[51]

For FPE, conduction is limited by emission from traps in the bulk of the oxide, where

$$I_{FPE} = V \exp\left[\frac{-q\left(\phi_T - \sqrt{qV/\pi\kappa_r\varepsilon_0}\right)}{kT}\right], \quad (3)$$

where ϕ_T is the trap energy depth referenced to the insulator conduction band minimum.[49] To determine whether the dominant conduction mechanism is related to FPE, the high field J-V data from Fig. 3(a) replotted as ln (I_{FPE}/V) vs. $V^{1/2}$ in Fig. 6. It is seen that the 10 nm thick ZrO_2, Ta_2O_5, and Nb_2O_5 devices produce linear fits in the FPE plots with $R^2 > 0.999$, suggesting that FPE is the dominate conduction mechanism for these devices. For SiO_2 and Al_2O_3, the linearity was poor ($R^2 < 0.98$), consistent with our tentative assignment of FNT dominated conduction for these devices. The linearity of the HfO_2 devices, on the other hand, was characterized by $R^2 = 0.997$, suggesting that in addition to FNT, thermal conduction mechanisms also play a role.

To assess the validity of the tentative FPE assignment for Nb_2O_5, Ta_2O_5, and ZrO_2, the dynamic relative dielectric constants, κ_r, are extracted from the slopes of the plots in Fig. 6. For Ta_2O_5, Nb_2O_5, and ZrO_2, the extracted values of κ_r are 4.6 ± 0.1, 5.5 ± 0.1, and 4.4 ± 0.1, respectively. Note that the values of κ_r are essentially the same for both polarities. Although it is clear that all of these extracted dielectric constants are much smaller than the static dielectric constant κ measured via C-V and shown in Table I, it is the optical dielectric constant to which they should be compared.[52–54] The optical dielectric constant for each material was estimated from the refractive index, n, which was measured in the wavelength range of 400–1200 nm using spectroscopic ellipsometry. As summarized in Table I, n^2 was measured to range from 5.5 to 6.2 for Nb_2O_5, from 4.6 to 4.95 for Ta_2O_5, and from 4.5 to 4.9 for ZrO_2. The κ_r values extracted from the FPE plots (5.5 ± 0.1 for Nb_2O_5, 4.6 ± 0.1 for Ta_2O_5, and 4.4 ± 0.1 for ZrO_2), are all at the low end of the range of values measured optically, supporting the assignment of FPE as the dominant mechanism at high fields in these films.

[This article is copyrighted as indicated in the article. Reuse of AIP content is subject to the terms at: http://scitation.aip.org/termsconditions. Downloaded to] IP: 128.193.38.25 On: Mon, 14 Jul 2014 16:34:45

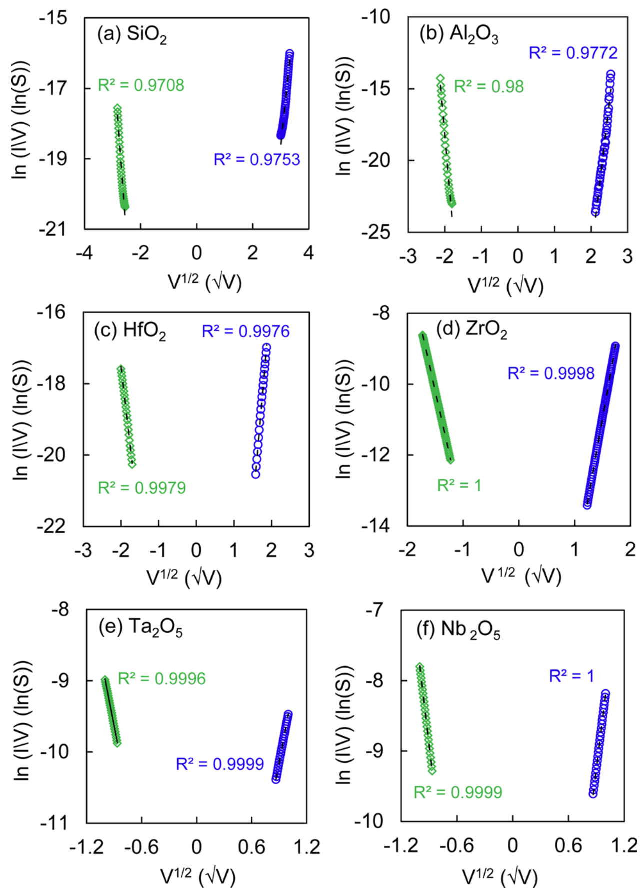

FIG. 6. I-V curves from Fig. 3(a) fitted to Frenkel-Poole plots (ln (I/V) vs. $V^{1/2}$). The voltage fitting range for each insulator is the same as in the FNT plots shown in Fig. 5. Green and blue curves represent negative and positive polarities, respectively. Curves showing $R^2 \geq 0.999$ are considered to be highly linear and exhibiting Frenkel-Poole emission as the dominant conduction mechanism.

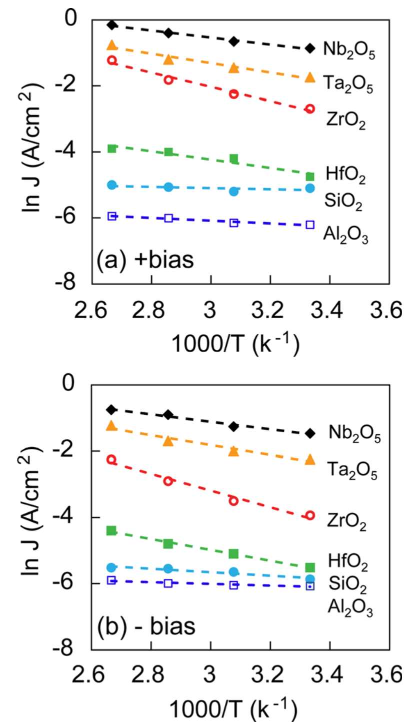

FIG. 7. Plots of log(J) vs. 1000/T illustrating the temperature dependence of the (a) positive and (b) negative bias current response for M_1IM_2 diodes made with 10 nm of either SiO_2, Al_2O_3, HfO_2, ZrO_2, Ta_2O_5, or Nb_2O_5. The magnitude of the applied bias for each device is chosen so that the current density is larger than 1 μA/cm^2.

Through simple fitting of I-V curves, FPE and FNT have been tentatively identified as dominant conduction mechanisms in these devices. Studying conduction in thin film insulators based solely on room temperature I-V data, however, can produce misleading results. Additional clarification of conduction mechanisms in thin dielectrics is accomplished by examining I-V behavior at different temperatures. To further distinguish between temperature independent and temperature dependent conduction mechanisms, MIM diode I-V characteristics were measured at 25, 50, 75, and 100 °C. Boltzmann plots of ln(J) vs. 1000/T illustrating the temperature dependence are shown in Fig. 7. The magnitude of the applied bias for each device is chosen so that the current density is larger than 1 μA/cm^2. Boltzmann plots are considered for both (a) positive applied bias (electron injection from ZrCuAlNi bottom electrode) and (b) negative applied bias (electron injection from Al top electrode) in order to identify the influence of electrodes and the electrode/insulator interfaces in conduction processes. According to Eq. (1) tunneling should be independent of temperature, to first order. Therefore, conduction in MIM diodes dominated by tunneling should exhibit only a weak dependence on temperature. It is seen in Fig. 7 that conduction in both the SiO_2 and Al_2O_3 devices is roughly independent of temperature, confirming the tentative assignment of tunneling as the dominant conduction mechanism in these devices. On the other hand, the ZrO_2, Ta_2O_5, and Nb_2O_5 diodes all exhibit strong temperature dependence at both positive and negative bias, confirm that thermal emission mechanisms play a strong role and suggesting that FPE is indeed the dominant mechanism in these devices.

The HfO_2 devices also demonstrate temperature dependence, further indicating that conduction in these devices is not simply dominated by FNT. Previous studies of ALD HfO_2 films have established TAT and FPE as the dominant conduction mechanisms.[53–55] Thus, the strong temperature dependence exhibited by the HfO_2 devices combined with the excellent linearity in the FNT plot (Fig. 5(c)) may be explained by TAT. The opposite polarity asymmetry ($\eta_{asym.} < 1$) exhibited by the HfO_2 diodes in Fig. 4(a) might also be explained by TAT filling of FPE defects. The probability of TAT is higher when defects are located close to the injecting interface (cathode). We have discussed previously that, due to the presence of a native oxide on the ZCAN electrode, the defect density should be larger near the ZCAN/HfO_2 interface than near the Al/HfO_2 interface.[16,27] Thus, TAT should be more favored under positive applied bias (electron injection from the ZCAN bottom electrode). The $\eta_{asym.} < 1$ measured for HfO_2 diodes implies larger current at positive polarity than for negative polarity, consistent with the above argument for TAT filling of defects.

Individual log(J)-V curves as a function of temperature are shown in Fig. 8 for (a) ZrO_2 and (b) Al_2O_3. For the ZrO_2 diodes in Fig. 8(a), the dramatic appearance of the knees in

[This article is copyrighted as indicated in the article. Reuse of AIP content is subject to the terms at: http://scitation.aip.org/termsconditions. Downloaded to] IP: 128.193.38.25 On: Mon, 14 Jul 2014 16:34:45

the 150 K curve indicates a shift in the dominant conduction mechanism from FPE at higher temperatures to FNT at lower temperature. This data clearly demonstrate that at low temperatures, FPE is shut down, trapped electrons no longer have enough energy to escape to the conduction band, and conduction becomes limited by FNT.

For the Al_2O_3 device in Fig. 8(b), it is seen that conduction is only weakly dependent upon temperature, confirming the domination of FNT. Note that slight changes (sharpening of the knees) in I-V response over a 300 K difference in temperature as defect and thermal based conduction processes that also contribute to conduction are frozen out. These relatively minor contributions are eliminated at 150 K and below so that at 78 K and 150 K, the Al_2O_3 diodes show sharp turn-on characteristics.

FPE may be thought of as being limited by transport through a dominant trap. The activation energy, E_a, required to escape from this trap at a given applied voltage may be extracted from Arrhenius plots of ln (I/V) vs. 1/kT like the one shown in Fig. 9 for the ZrO_2 devices. Using these field dependent E_a values, the energy depth of the dominant trap, ϕ_T, in reference to the conduction band minimum of the insulator may be estimated for the insulators dominated by FPE. To account for the Schottky barrier lowering of the trap depth when a field is applied across the insulator, the obtained values of E_a are plotted vs. the square root of the voltage drop across the insulator, as shown in Fig. 10. ϕ_T is then estimated by extrapolating to V = 0. For Nb_2O_5, Ta_2O_5, and ZrO_2, ϕ_T was estimated to be 0.62 ± 0.05 eV, 0.53 ± 0.05 eV, and 1.65 ± 0.1 eV below the conduction band minimum, respectively. The extracted trap depths were the same for both positive and negative biases, further evidence that FPE is indeed dominant in this bias region. These extracted values are in reasonable agreement with the reported values for these insulators deposited with ALD. Using $TaCl_5$ as the precursor, Houssa *et al.* have reported $\phi_T = 0.7$ eV for Ta_2O_5 films.[44] García *et al.* have recently reported $\phi_T = 0.8$ eV for annealed Nb_2O_5 films deposited by PEALD with $Nb(Net_2)_3$.[46] ZrO_2 defect levels have been reported to be between 2 and 2.5 eV below conduction band.[32]

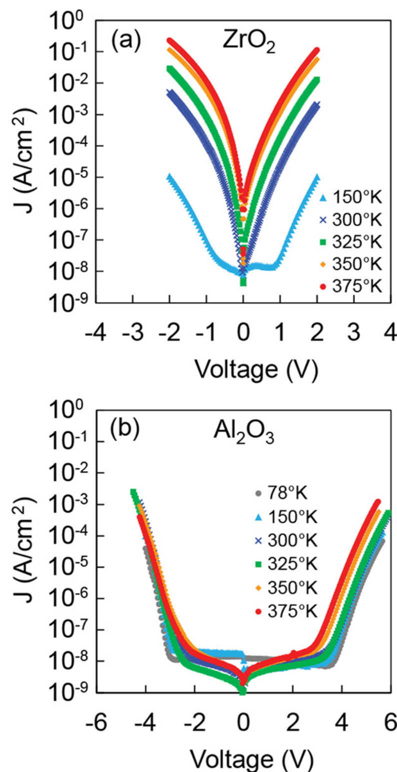

FIG. 8. Plots of current density (J) vs. V as a function of temperatures for M_1IM_2 diodes 10 nm thick insulator layers of either (a) ZrO_2 or (b) Al_2O_3.

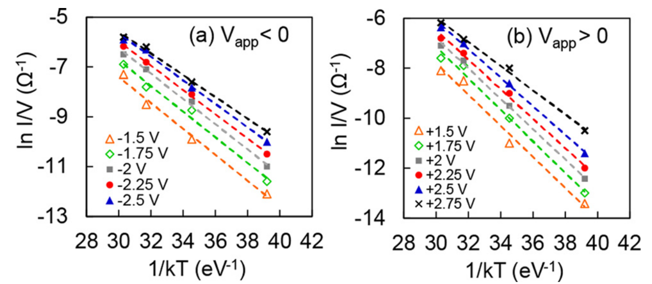

FIG. 9. Arrhenius plots of I/V vs. 1/kT of a series of (a) negative and (b) positive voltages above V_{ON} for a ZrO_2 device. The slopes of the curves are used to extract the voltage dependent activation energies which are plotted vs. sqrt(V) in Fig. 10 to determine ϕ_T.

C. Discussion on the choice of insulators

Trap energies are summarized in Table I. Comparing the electrically extracted trap energies to the oxygen vacancy levels measured via REELS, it is seen that the values are qualitatively consistent, suggesting that the oxygen vacancy related defects in the upper half of the bandgaps may be responsible for FPE in Nb_2O_5, Ta_2O_5, and ZrO_2. Shown in Fig. 11 are energy band diagram sketches of all the insulators investigated in this work with both electrically determined defect levels and REELS measured intrinsic oxygen vacancy related defect levels indicated. The interplay between electrode work function and insulator band-gap, electron affinity, defect levels, and defect density determine the suitability of an insulator for a potential application. For the low electron affinity oxides, SiO_2 and Al_2O_3, the trap levels in the upper part of the band gaps are well above the Fermi level of the electrodes and thus do not get a chance to play a dominant role in conduction. The deeper REELS level (3.8 eV) detected in SiO_2 is too deep for FPE to be significant but appears to contribute to increased leakage at low fields via TAT. On the other hand, for medium electron affinity insulator with fairly deep trap levels (HfO_2 and ZrO_2), as well as for high electron affinity insulators with shallow defect levels (Nb_2O_5 and Ta_2O_5), the defects are located energetically in the vicinity of the electrode Fermi levels allowing them to play a dominant role in conduction. These oxides tend to be dominated by defect related conduction mechanisms such as FPE and TAT. Thus, one cannot simply choose an insulator for an application based solely on say electron affinity.

A close inspection of the ZrO_2, Ta_2O_5, and Nb_2O_5 asymmetry vs. voltage curves in Fig. 4(a) reveals a slightly asymmetric I-V response in low bias range. As we have shown elsewhere,[51] this asymmetry is due to dominance of electrode limited SE at low biases. The fairly small energy barriers that

[This article is copyrighted as indicated in the article. Reuse of AIP content is subject to the terms at: http://scitation.aip.org/termsconditions. Downloaded to] IP: 128.193.38.25 On: Mon, 14 Jul 2014 16:34:45

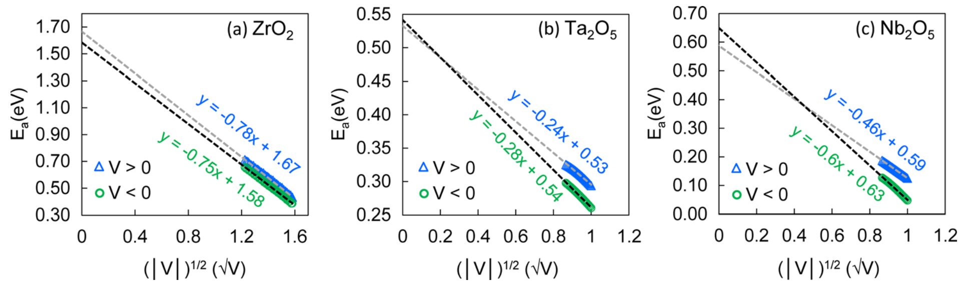

FIG. 10. Plots of E_a vs. sqrt|V| in the FPE dominated bias regime ($V_{appl} > 0.7$ V) for (a) 10 nm ZrO_2 diodes, (b) 10 nm Ta_2O_5, and (c) 10 nm Nb_2O_5 diodes. The trap depth, ϕ_{T0}, is extracted by extrapolation of the curves to zero bias. All the curves used for extrapolating trap depths are linear with $R^2 > 0.99$.

Ta_2O_5, and Nb_2O_5, and even ZrO_2 form with the electrodes allows for electrons to surmount this barrier in the low bias regime, resulting in SE leakage. At high biases, conduction becomes dominated by emission from traps in the insulator. As SE is strongly temperature dependent, the transition bias between electrode limited SE and bulk limited FPE and thus the asymmetry are also strongly temperature dependent.

In order to obtain strong asymmetric I-V characteristics, conduction in an MIM structure should be dominated by an electrode limited mechanism such as FNT or SE.[13] (As a bulk-limited conduction mechanism, FPE cannot provide large asymmetry as the traps that dominate conduction behave the same under both polarities.) If temperature insensitive operation is desired, the strongly temperature dependent SE mechanism should be avoided. We have demonstrated that the choice of insulator is thus critical in determining MIM diode performance and suitability for a given application. Although SiO_2, and Al_2O_3, and perhaps HfO_2 may be suitable for applications such as selector diodes for RRAM or LCD backplanes, for IR detection or IR energy harvesting applications that require low voltage operation, insulators with low electron affinities such as Nb_2O_5 and Ta_2O_5 appear to be attractive. However, we have shown that due to their small band offsets (tunnel barriers), low electron affinity insulators will tend to be dominated by thermal emission mechanisms, in particular, FPE, and thus exhibit low asymmetry.[51]

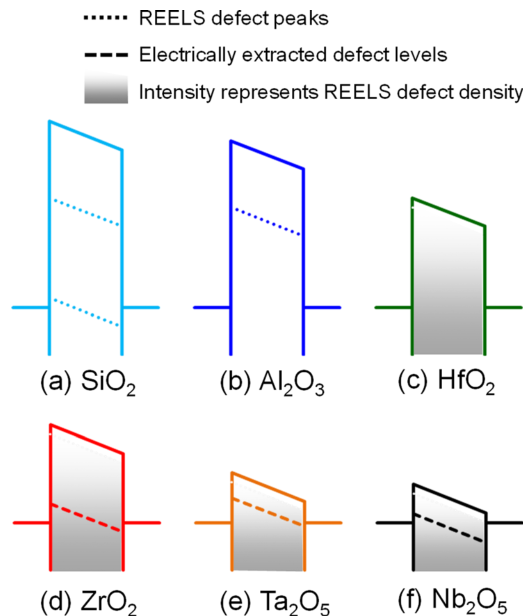

FIG. 11. Equilibrium energy band diagrams with defect levels indicated. Dotted lines in (a) SiO_2 and (b) Al_2O_3 indicate distinct energy levels peaks determined by REELS. The shaded region in (c) HfO_2, (d) ZrO_2, (e) Ta_2O_5, and (f) Nb_2O_5 represents the extended range of oxygen vacancy related defect levels as determined by REELS. Darker shading is meant to represent higher densities of defects. Finally, the thick dashed lines in (d) ZrO_2, (e) Ta_2O_5, and (f) Nb_2O_5 indicate defect levels extracted from electrical measurements.

So what are the strategies then for engineering MIM devices with low V_{ON} and high asymmetry? It has been discussed that if the insulator thickness is reduced, a transition in dominant conduction mechanism from a bulk limited to electrode limited should occur.[4,13,49] Thus, decreasing the thickness of the insulator layer would seem to be a viable strategy to enhance asymmetry of M_1IM_2 tunnel diodes. We have shown previously that dissimilar electrode MIM diodes can have smaller V_{ON} as well as exhibit significant asymmetry and non-linearity at lower biases as the insulator is thinned.[27] However, MIM diodes dominated by FNT exhibit lower η_{max} and reduced $f_{NL\text{-}max}$ as insulator thickness is reduced. For example, Al_2O_3 diodes made with 12 (∼5 Å) and 16 (∼10 Å) ALD cycles are almost symmetric.[16] The small asymmetry values for diodes made with thinner insulators are due to an increase in the contribution of direct tunneling to conduction.

Another strategy to improve I-V asymmetry in tunnel diodes is the use of nanolaminate insulator stacks.[4,27,56–58] Recently, we showed that a nanolaminate pair of insulators (Al_2O_3/HfO_2) can be used to form metal-insulator-insulator-metal (MIIM) diodes with enhanced performance over single layer MIM diodes and demonstrated that the observed enhancements in low voltage asymmetry are due to "step tunneling," a situation in which an electron may tunnel through only the larger band-gap insulator instead of both.[27] Narrow band-gap dielectrics, such as Ta_2O_5 and Nb_2O_5, are attractive for MIM diodes because the small barrier heights allow for low turn-on voltages. However, because conduction is based on temperature sensitive emission, rather than tunneling, devices based on single layers of these materials may not be suitable for stable high speed rectification. For MIIM diodes based on step tunneling, only one of the dielectrics may be required to be dominated by tunneling. Using MIIM structures, narrow band-gap dielectrics dominated by thermal emission may be combined with wider band-gap dielectrics dominated by tunneling to enable low turn-on voltage high asymmetry tunnel diodes.[59]

IV. SUMMARY/CONCLUSION

In summary, whereas past thin film diode work has focused on oxides or nitrides of an underlying polycrystalline metal electrode, in this work we investigate MIM diodes with a wide range of insulators and a single set of metal electrodes. Nb_2O_5, Ta_2O_5, ZrO_2, HfO_2, Al_2O_3, and SiO_2 were

[This article is copyrighted as indicated in the article. Reuse of AIP content is subject to the terms at: http://scitation.aip.org/termsconditions. Downloaded to] IP: 128.193.38.25 On: Mon, 14 Jul 2014 16:34:45

deposited via ALD on atomically smooth amorphous ZrCuAlNi bottom electrodes with Al top electrodes. To preserve the amorphous structure of metals and insulators, no annealing was performed. MIM diode performance, including current vs. voltage asymmetry and non-linearity, is compared. Dominant conduction mechanisms in these tunnel barriers are identified by analyzing plots of current density (J) versus V at temperatures ranging from 78 K to 375 K. The band-gap energy and energy position of intrinsic sub-gap defect states for each of the insulators are measured using REELS.

It is found that for low electron affinity insulators with intrinsic defect levels well above the electrode Fermi levels, such as SiO_2 and Al_2O_3, conduction at high fields is dominated by FNT. These diodes offer the highest maximum I-V asymmetry (>1000X for Al_2O_3 and 10X for SiO_2) and non-linearity values, but require relatively high V_{ON}. In the high electron affinity insulators investigated, Nb_2O_5 and Ta_2O_5, shallow defects near the metal Fermi levels allow conduction to be dominated by FPE in the high bias regime. Electrical estimates of FPE trap energy levels are found to be consistent with the REELS measurements of oxygen vacancy energy levels in Nb_2O_5, Ta_2O_5, and ZrO_2. Nb_2O_5 and Ta_2O_5 devices offer the lowest V_{ON}, but low I-V asymmetry (<2X). The intermediate electron affinity insulators, HfO_2 and ZrO_2, have deeper intrinsic trap levels located energetically near the metal Fermi level and conduction is found to be a mixture of FPE and tunneling. ZrO_2 is dominated by FPE at room temperature and above and FNT at 150 K and below. HfO_2 is dominated by tunneling but has a strong temperature dependent FPE component. HfO_2 and ZrO_2 show intermediate V_{ON} and maximum asymmetry close to 10X.

In conclusion, we investigated the impact of the tunnel insulator material on MIM diode performance using a fixed pair of metal electrodes and a variety of high and low electron affinity as-deposited ALD insulators. We find that the details of the insulator, including electron affinity, bandgap, and band offsets, along with defect levels and defect density are critical in determining MIM diode performance and suitability for a particular application.

ACKNOWLEDGMENTS

This work was supported in part by grants from the National Science Foundation through DMR-0805372 with matching support from the Oregon Nanoscience and Microtechnologies Institute (ONAMI). The authors thank Professor J. F. Wager and John McGlone of OSU for ZCAN films, Ram Ravichandran for performing spectroscopic ellipsometry, Mark Sowa of Cambridge Nanotech for PE-ALD SiO_2 films, and Chris Tasker of the OSU Materials Synthesis and Characterization (MaSC) Facility for equipment support.

[1]S. Vaziri, G. Lupina, C. Henkel, A. D. Smith, M. Östling, J. Dabrowski, G. Lippert, W. Mehr, and M. C. Lemme, Nano Lett. **13**(4), 1435 (2013).
[2]C. Zeng, E. B. Song, M. Wang, S. Lee, C. M. Torres, Jr., J. Tang, B. H. Weiller, and K. L. Wang, Nano Lett. **13**(6), 2370 (2013).
[3]N. M. Miskovsky, P. H. Cutler, A. Mayer, B. L. Weiss, B. Willis, T. E. Sullivan, and P. B. Lerner, J. Nanotechnol. **2012**, 1–19 (2012).
[4]*Rectenna Solar Cells*, edited by G. M. Moddel and S. Grover (Springer, New York, 2013).
[5]P. C. D. Hobbs, R. B. Laibowitz, F. R Libsch, N. C. LaBianca, and P. P. Chiniwalla, Opt. Express **15**(25), 16376 (2007).
[6]I. Codreanu, F. J. Gonzalez, and G. D. Boreman, Infrared Phys. Technol. **44**(3), 155 (2003).
[7]B. Govoreanu, C. Adelmann, A. Redolfi, L. Zhang, S. Clima, and M. Jurczak, IEEE Electron Device Lett. **35**(1), 63 (2014).
[8]R. D. Clark, Materials **7**, 2913 (2014).
[9]T. W. Hickmott, J. Appl. Phys. **108**, 093703 (2010).
[10]M. Suzuki, M. Sagawa, T. Kusunoki, E. Nishimura, M. Ikeda, and K. Tsuji, IEEE Trans. Electron Devices **59**, 2256 (2012).
[11]W. den Boer, *Active Matrix Liquid Crystal Displays* (Elsevier, Amsterdam, 2005), pp. 43–47.
[12]R. H. Reuss, B. R. Chalamala, A. Moussessian, M. G. Kane, A. Kumar, D. C. Zhang, J. A. Rogers, M. Hatalis, D. Temple, G. Moddel *et al.*, Proc. IEEE **93**(7), 1239 (2005).
[13]J. G. Simmons, J. Phys. D: Appl. Phys. **4**, 613 (1971).
[14]C. W. Miller, Z. Li, J. Åkerman, and I. K. Schuller, Appl. Phys. Lett. **90**, 043513 (2007).
[15]N. Alimardani, J. F. Conley, Jr., E. W. Cowell III, J. F. Wager, M. Chin, S. Kilpatrick, and M. Dubey, in Proceedings of IEEE International Integrated Reliability Workshop (IRW) Final Report (2010), pp. 80–84.
[16]E. E. Cowell III, N. Alimardani, C. C. Knutson, J. F. Conley, Jr., D. A. Keszler, B. J. Gibbons, and J. F. Wager, Adv. Mater. **23**(1), 74 (2011).
[17]N. Alimardani, E. W. Cowell III, J. F. Wager, J. F. Conley, Jr., D. R. Evans, M. Chin, S. J. Kilpatrick, and M. Dubey, J. Vac. Sci. Technol., A **30**(1), 01A113 (2012).
[18]C. B. Duke, *Tunneling in Solids* (Academic Press, New York, 1969), Chap. 5, p. 90.
[19]H. Ekurt and A. Hahn, J. Appl. Phys. **51**, 1686 (1980).
[20]P. Periasamy, J. J. Berry, A. A. Dameron, J. D. Bergeson, D. S. Ginley, R. P. O'Hayre, and P. A. Parilla, Adv. Mater. **23**, 3080 (2011).
[21]F. Miao, J. P. Strachan, J. J. Yang, M.-X. Zhang, I. Goldfarb, A. C. Torrezan, P. Eschbach, R. D. Kelley, G. Medeiros-Ribeiro, and R. S. Williams, Adv. Mater. **23**(47), 5633 (2011).
[22]K.-L. Lin, T.-H. Hou, J. Shieh, J.-H. Lin, C.-T. Chou, and Y.-J. Lee, J. Appl. Phys. **109**, 084104 (2011).
[23]V. Miikkulainen, M. Leskelä, M. Ritala, and R. L. Puurunen, J. Appl. Phys. **113**, 021301 (2013).
[24]P. Sharma, N. Kaushik, H. Kimura, Y. Saotome, and A. Inoue, Nanotechnology **18**, 035302 (2007).
[25]T. Usui, S. A. Mollinger, A. T. Iancu, R. M. Reis, and F. B. Prinz, Appl. Phys. Lett. **101**, 033905 (2012).
[26]K. Choi, F. Yesilkoy, G. Ryu, S. H. Cho, N. Goldsman, M. Dagenais, and M. Peckerar, IEEE Trans. Electron Devices **58**(10), 3519 (2011).
[27]N. Alimardani and J. F. Conley, Jr., Appl. Phys. Lett. **102**, 143501 (2013).
[28]S. King, M. French, M. Jaehnig, M. Kuhn, B. Boyanov, and B. French, J. Vac. Sci. Technol., B **29**, 51207 (2011).
[29]S. W. King, B. French, and E. Mays, J. Appl. Phys. **113**, 044109 (2013).
[30]R. G. Southwick III, A. Sup, A. Jain, and W. B. Knowlton, IEEE Trans. Device Mater. Reliab. **11**(2), 236 (2011).
[31]B. L. French and S. W. King, J. Mater. Res. **28**(20), 2771 (2013).
[32]C. Morant, A. Fernández, A. R. González-Elipe, L. Soriano, A. Stampfl, A. M. Bradshaw, and J. M. Sanz, Phys. Rev. B **52**, 11711 (1995).
[33]J. Robertson, Rep. Prog. Phys. **69**, 327 (2006).
[34]A. Foster, F. Lopez Gejo, A. Shluger, and R. Nieminen, Phys. Rev. B **65**, 174117 (2002).
[35]A. Foster, V. Sulimov, F. Lopez Gejo, A. Shluger, and R. Nieminen, J. Non-Cryst. Solids **303**, 101 (2002).
[36]Z. Xu, M. Houssa, S. De Gendt, and M. Heyns, Appl. Phys. Lett. **80**, 1975 (2002).
[37]S. Monaghan, P. K. Hurley, K. Cherkaoui, M. A. Negara, and A. Schenk, Solid-State Electron. **53**(4), 438 (2009).
[38]G. Ribes, S. Bruyere, D. Roy, C. Parthasarthy, M. Muller, M. Denais, V. Huard, T. Skotnicki, and G. Ghibaudo, IEEE Trans. Device Mater. Reliab. **6**, 132 (2006).
[39]A. Kerber and E. Cartier, IEEE Trans. Device Mater. Reliab. **9**, 147 (2009).
[40]H. Sawada and K. Kawakami, J. Appl. Phys. **86**, 956 (1999).
[41]R. Bondi, M. Desjarlais, A. Thompson, G. Brennecka, and M. Marinella, J. Appl. Phys. **114**, 203701 (2013).
[42]D. Hiller, R. Zierold, J. Bachmann, M. Alexe, Y. Yang, J. W. Gerlach, A. Stesmans, M. Jivanescu, U. Müller, J. Vogt *et al.*, J. Appl. Phys. **107**, 064314 (2010).

[This article is copyrighted as indicated in the article. Reuse of AIP content is subject to the terms at: http://scitation.aip.org/termsconditions. Downloaded to] IP: 128.193.38.25 On: Mon, 14 Jul 2014 16:34:45

[43]S. Swaminathan, Y. Sun, P. Pianetta, and P. C. McIntyre, J. Appl. Phys. **110**, 094105 (2011).
[44]M. Houssa, M. Tuominen, M. Naili, V. Afanas'ev, A. Stesmans, S. Haukka, and M. M. Heyns, J. Appl. Phys. **87**, 8615 (2000).
[45]J. Robertson, J. Vac. Sci. Technol., B **18**, 1785 (2000).
[46]H. García, H. Castán, E. Perez, S. Dueñas, L. Bailón, T. Blanquart, J. Niinistö, M. Ritala, and M. Leskelä, Semicond. Sci. Technol. **28**, 055005 (2013).
[47]S. W. Smith, K. McAuliffe, and J. F. Conley, Jr., Solid State Electron. **54**, 1076 (2010).
[48]Y.-C. Yeo, T.-J. King, and C. Hu, J. Appl. Phys. **92**(12), 7266 (2002).
[49]S. M. Sze and K. K. Ng, *Physics of Semiconductor Devices*, 3rd ed. (Hoboken, NJ: Wiley-Interscience, 2007).
[50]A. Rose, Phys. Rev. **97**, 1538 (1955).
[51]N. Alimardani, J. M. McGlone, J. F. Wager, and J. F. Conley, Jr., J. Vac. Sci. Technol., A **32**(1), 01A122(2014).
[52]M. Specht, M. Stadele, S. Jakschik, and U. Schroder, Appl. Phys. Lett. **84**, 3076 (2004).
[53]D. S. Jeong and C. S. Hwang, J. Appl. Phys. **98**, 113701 (2005).
[54]Ch. Walczyk, Ch. Wenger, R. Sohal, M. Lukosius, A. Fox, J. Dąbrowski, D. Wolansky, B. Tillack, H.-J. Müssing, and T. Schroeder, J. Appl. Phys. **105**, 114103 (2009).
[55]S. Yu, X. Guan, and H.-S. Philip Wong, Appl. Phys. Lett. **99**, 063507 (2011).
[56]P. A. Schulz and C. E. T. Gonçalves da Silva, Appl. Phys. Lett. **52**(12), 960 (1988).
[57]M. Di Ventra, G. Papa, C. Coluzza, A. Baldereschi, and P. A. Schulz, J. Appl. Phys. **80**(7), 4174 (1996).
[58]P. Maraghechi, A. Foroughi-Abari, K. Cadien, and A. Y. Elezzabi, Appl. Phys. Lett. **100**, 113503 (2012).
[59]N. Alimardani and J. F. Conley, Jr., "Enhancing metal-insulator-insulator-metal (MIIM) tunnel diodes by defect enhanced direct tunneling" (submitted).

[This article is copyrighted as indicated in the article. Reuse of AIP content is subject to the terms at: http://scitation.aip.org/termsconditions. Downloaded to] IP: 128.193.38.25 On: Mon, 14 Jul 2014 16:34:45